Direct measurement of the near-field super resolved focused spot in InSb

A.C. Assafrao,[1,*] **A.J.H. Wachters,**[1] **M. Verheijen,**[1] **A.M. Nugrowati,**[1] **S.F. Pereira,**[1] **H.P. Urbach,**[1] **Marie-Francoise Armand,**[2] **and Segolene Olivier**[2]

[1] *Optics Research Group, Department of Imaging Science and Technology, Delft University of Technology, Lorentzweg 1, 2628 CJ Delft, The Netherlands*

[2] *CEA-Leti, Minatec Campus, 17 rue des Martyrs, 38054 Grenoble Cedex 9, France*

[*] *a.dacostaassafrao@tudelft.nl*

Abstract: Under appropriate laser exposure, a thin film of InSb exhibits a sub-wavelength thermally modified area that can be used to focus light beyond the diffraction limit. This technique, called Super-Resolution Near-Field Structure, is a potential candidate for ultrahigh density optical data storage and many other high-resolution applications. We combined near field microscopy, confocal microscopy and time resolved pump-probe technique to directly measure the induced sub-diffraction limited spot in the near-field regime. The measured spot size was found to be dependent on the laser power and a decrease of 25% (100nm) was observed. Experimental evidences that support a threshold-like simulation model to describe the effect are also provided. The experimental data are in excellent agreement with rigorous simulations obtained with a three dimensional Finite Element Method code.

OCIS codes: (210.0210) Optical data storage; (210.4245) Near-field optical recording

References and links

1. D. W. Pohl, W. Denk, and M. Lanz, "Optical stethoscopy: Image recording with resolution lambda/20," Appl. Phys. Lett. **44**, 651–653 (1984).
2. M. Kuwahara, T. Nakano, J. Tominaga, M. B. Lee, and N. Atoda, "High-speed optical near-field photolithography by super resolution near-field structure," Jpn. J. Appl. Phys. **38**, L1079–L1081 (1999).
3. E. Betzig, S. G. Grubb, R. J. Chichester, D. J. DiGiovanni, and J. S. Weiner, "Fiber laser probe for near-field scanning optical microscopy," Appl. Phys. Lett. **63**, 3550–3552 (1993).
4. I. Ichimura, S. Hayashi, and G. S. Kino, "High-density optical recording using a solid immersion lens," Appl. Opt. **36**, 4339–4348 (1997).
5. W. H. Yeh and M. Mansuripur, "Evanescent coupling in magneto-optical and phase-change disk systems based on the solid immersion lens," Appl. Opt. **39**, 302–315 (2000).
6. J. Tominaga, T. Nakano, and N. Atoda, "An approach for recording and readout beyond the diffraction limit with an sb thin film," Appl. Phys. Lett. **73**, 2078–2080 (1998).
7. J. Tominaga, H. Fuji, A. Sato, T. Nakano, and N. Atoda, "The characteristics and the potential of super resolution near-field structure," Jpn. J. Appl. Phys. **39**, 957–961 (2000).
8. J. Pichon, R. Anciant, J. M. Bruneau, B. Hyot, S. Gidon, M. F. Armand, and L. Poupinet, "Multiphysics simulation of super-resolution bd rom optical disk readout," SPIE **6282**, 628219 (2006).
9. K. Nakai, M. Ohmaki, N. Takeshita, B. Hyot, B. André, and L. Poupinet, "Bit-error-rate evaluation of super-resolution near-field structure read-only memory discs with semiconductive material insb," Jpn. J. Appl. Phys. **49**, 08KE01 (2010).
10. K. Nakai, M. Ohmaki, N. Takeshita, M. Shinoda, I. Hwang, Y. Lee, H. Zhao, J. Kim, B. Hyot, B. André, L. Poupinet, T. Shima, T. Nakano, and J. Tominaga, "First playback of high-definition video contents from super-resolution near-field structure optical disc," Jpn. J. Appl. Phys. **49**, 08KE02 (2010).

#162345 - $15.00 USD Received 1 Feb 2012; revised 24 Feb 2012; accepted 24 Feb 2012; published 20 Apr 2012

11. R. E. Simpson, P. Fons, X. Wang, A. V. Kolobov, T. Fukaya, and J. Tominaga, "Non-melting super-resolution near-field apertures in sb–te alloys," Appl. Phys. Lett. **97**, 161906 (2010).
12. S. Ohkubo, K. Aoki, and D. Eto, "Temperature dependence of optical constants for insb films including molten phases," Appl. Phys. Lett. **92**, 011919 (2008).
13. M. Kuwahara, T. Shima, A. Kolobov, and J. Tominaga, "Thermal origin of readout mechanism of light-scattering super-resolution near-field structure disk," Jpn. J. Appl. Phys. **43**, L8–L10 (2004).
14. T. Shima, M. Kuwahara, T. Fukaya, T. Nakano, and J. Tominaga, "Super-resolutional readout disk with metal-free phthalocyanine recording layer," Jpn. J. Appl. Phys. **43**, L88–L90 (2004).
15. J. S. Kim, K. Kwak, and C.Y. You, "Signal modulation of super read only memory with thermally activated aperture model," Jpn. J. Appl. Phys. **47**, 5845–5847 (2008).
16. A. C. Assafrao, S. F. Pereira, H. P. Urbach, C. Fery, L. von Riewel, and S. Knappmann, "A numerical model for superresolution effect in optical discs," SPIE **7730**, 77301J (2010).
17. G. Pilard, C. Féry, L. Pacearescu, H. Hoelzemann and S. Knappmann, "Study of super-resolution read-only-memory disk with a semiconducting or chalcogenide mask layer," Jpn. J. Appl. Phys. **48**, 03A064 (2009).
18. J. Tominaga, J. Kim, H. Fuji, D. Büchel, T. Kikukawa, L. Men, H. Fukuda, A. Sato, T. Nakano, A. Tachibana, Y. Yamakawa, M. Kumagai, T. Fukaya, and N. Atoda, "Super-resolution near-field structure and signal enhancement by surface plasmons," Jpn. J. Appl. Phys. **40**, 1831–1834 (2001).
19. A. C. Assafrao, S. F. Pereira, and H. P. Urbach, "Scalar readout model for super-rens focused spot," J. Europ. Opt. Soc. Rap. Public. **6**, 11056 (2011).
20. T. Fukaya, D. Büchel, S. Shinbori, J. Tominaga, N. Atoda, D. P. Tsai, and W. C. Lin, "Micro-optical nonlinearity of a silver oxide layer," J. Appl. Phys. **89**, 6139–6144 (2001).
21. M. Franko and C. D. Tran, "Analytical thermal lens instrumentation," Rev. Sci. Inst. **67**, 1–18 (1996).
22. A. J. Wachters and H. P. Urbach, "Finite-element model for electromagnetic scattering problems," Technical Note Phillips Research Europe , PR-TN 00042 (2008).
23. X. Wei, A. J. Wachters, and H. P. Urbach, "Finite-element model for three-dimensional optical scattering problems," J. Opt. Soc. Am. A **24**, 866–881 (2007).
24. J. Pichon, "Super-resolution optical data storage," Thesys (2009).
25. A. C. Assafrao, S. F. Pereira and H. P. Urbach, "On the focused field embedded in a super rens medium," Jpn. J. Appl. Phys. **50**, 102206 (2011).
26. M. Kuwahara, O. Suzuki, N. Taketoshi, Y. Yamakawa, T. Yagi, P. Fons, K. Tsutsumi, M. Suzuki, T. Fukaya, J. Tominaga, and T. Baba, "Measurements of temperature dependence of optical and thermal properties of optical disk materials," Jpn. J. Appl. Phys. **45**, 1419–1421 (2006).

1. Introduction

In order to break the fundamental diffraction limit in optical systems, many techniques based on near-field optics have been proposed in the past years. By restoring the information carried by evanescent fields, otherwise lost during propagation, resolution beyond the diffraction limit can be achieved. These techniques immediately find their applications in areas such as microscopy [1], lithography [2], and optical data storage (ODS). For ODS applications, any attempt to retrieve evanescent information must be done in the vicinity of a fast spinning optical disc. Therefore, techniques which require a near field probe to be kept within nanometer distance from the rotating disc will face major issues regarding rigorous distance control systems. This applies to both near field optical recording [3] and optical recording using a solid immersion lens [4, 5]. To overcome these difficulties, a completely different approach has been proposed by Tominaga et al. [6, 7]. In the so called Super-REsolution Near-field Structure technique (Super-RENS), the focused laser beam induces a reversible subwavelength optical aperture in a thin layer of a Sb-based phase-change material close to the data layer. Therefore, no major modification of the Blu-Ray readout system is required since the layer itself, by means of the optical aperture, works as the near-field probe. By using this technique, Tominaga was able to readout data marks far beyond the diffraction limit, with excellent carrier-to-noise ratio (CNR). More recently, the InSb semiconductor was proposed as an alternative material to develop high-capacity Super-RENS optical discs [8]. In contrast to phase-change materials, a reversible sub-wavelength optical scatterer is generated in the InSb layer upon laser radiation, as schematically represented in Fig. 1. In addition to excellent CNR values, a very low bit error rate in the range of 10^{-5} (much better than the 3×10^{-4} criterion holding for Blu-Rays) was

#162345 - $15.00 USD Received 1 Feb 2012; revised 24 Feb 2012; accepted 24 Feb 2012; published 20 Apr 2012

measured [9]. With this material, high-definition video playback from a Super-RENS 46 GB optical disc was demonstrated for the first time [10]. Despite the good results, the detailed underlying physical mechanism of the Super-RENS effect, created by heating a sub-wavelength area with the incident focused laser, still has to be fully explained. The most recent contribution in this direction was given by Simpson et al. for SbTe materials [11]. In their study, they demonstrated that thermal vibrations can disturb the p-orbital interaction present in the octahedral coordination of the crystalline Sb alloys, resulting in a local and reversible refractive index change. For the semiconductor InSb, the increase of the extinction coefficient is believed to be due to the decrease of the band gap energy E_g as function of the temperature, as demonstrated by Ohkubo et al. [12]. Hence, the Super-RENS technique is a very active field that has attracted many researchers, due to its advantages over other near field techniques [13–17].

From a practical point of view, it is essential to understand the effect of the opened optical aperture/scatterer on the profile and intensity of the focused laser spot, regardless of its cause. For the aperture-type of Super-RENS materials, the interaction of the optical aperture and the laser beam is expected to result in a local focused spot that is not limited by diffraction. In this way, readout of data marks beyond the diffraction limit is possible. On the other hand, for scatterer-type of Super-RENS materials, the effect of the optical scatterer on the focused spot is not so straightforward to interpret. In fact, it has been proposed that surface plasmons enhancement or the strong interaction of the evanescent scattered field with the underneath data marks are the main responsible mechanisms for the readout signal beyond the diffraction limit [18–20]. Thus, for this type of Super-RENS material, a direct measurement of the focused spot after its interaction with the local sub-wavelength scatterer will greatly improve the overall understanding of the readout mechanism. In addition, for further development of the Super-RENS technique, it is necessary to develop and validate a simulation model that accurately predicts the focused spot characteristics after its interaction with the induced optical aperture/scatterer. In this work, we aim to experimentally measure, in the near-field regime, the Super-RENS focused spot after being transmitted by a super-resolution layer containing an active scatterer-like InSb super resolution layer. Three experimental techniques were used for this purpose. The experimental conditions in which the Super-RENS effect takes place were investigated by a time resolved pump-probe technique, adapted from the Thermal Lens technique [21], and Confocal Microscopy in reflection. Near-field measurements of the focused spot were performed using a commercial SNOM microscope, in direct contact with the surface of the Super-RENS sample. Moreover, a phenomenological model supported by experimental evidences was developed and run by a rigorous three dimensional (3D) Finite Element Method (FEM) tool [22, 23] to account for the Super-RENS effect and the resulting modification of the focused spot profile. The paper is organized as follows: details of the experimental setups are described in §2, while in §3 we present preliminary experimental measurements. In §4 we describe the intensity threshold model of the Super-RENS effect. In §5 we show the near-field measurements of the Super-RENS focused spot and compare the results with the simulations. Conclusions of this work are given in §6.

2. Experimental setup

A schematic diagram of the experimental setup is shown in Fig. 2. A diode laser operating at 405 nm wavelength (Laser Components, CS4051205X) was connected to a pulse generator (Tabor Electronics, Model 8600). For the time resolved pump-probe measurements, the sample was mounted on a stage translator, placed in the focal plane of the 100 mm singlet lens. The modulated blue laser was used as the excitation and probe beam. A fast photodetector (FPD), connected to an oscilloscope (Rigol DS1302CA), was used to pick-up the signal transmitted through the sample. For confocal microscopy and near field measurements, the pulsed laser

#162345 - $15.00 USD Received 1 Feb 2012; revised 24 Feb 2012; accepted 24 Feb 2012; published 20 Apr 2012

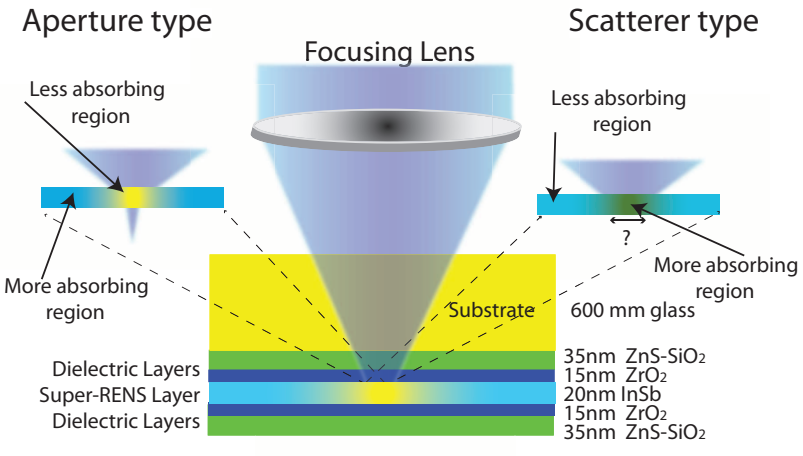

Fig. 1. Schematic representation of the aperture and scatterer types of Super-RENS effect. Under laser radiation, a sub-wavelength thermally induced region, smaller than the area of the focused spot, is generated in the super resolution layer. Within this region, the sample optical parameters (i.e., the permitivitty) are temporarily changed. For certain materials, the induced region (represented in yellow, on the left) becomes less absorbing than the outer region (blue). Therefore, an optical aperture is formed. For the InSb sample, the induced region (represented by green, on the right) becomes more absorbing than the outer region. Therefore, an optical scatterer is formed.

beam was coupled into a single mode fiber and redirected to the SNOM microscope (Witec Alpha 300S). Modifications were done in the SNOM scanning table to include a DVD lens (NA=0.6, corrected for 600μm glass plate), mounted on a 20μm piezo stage (Jena Mipos 20). The sample was placed in the focal region of the DVD lens. Near-field maps of the focused spot were taken in a $2 \times 2\mu$m^2 scanning window. To perform confocal microscopy in reflection, a red laser (Spectra-Physics He-Ne, $\lambda = 632$nm) was focused onto the sample through a high NA objective (Leitz Wetzlar NA$= 0.90/100$x). In this study, we used InSb-based Super-RENS samples, consisting of 5 layers of ZnS:SiO_2 35nm / ZrO_2 15nm / InSb 20nm / ZrO_2 15nm / ZnS:SiO_2 35nm, deposited on a 600μm glass substrate by magnetron sputtering. A sample consisting of 35nm ZnS:SiO_2 was also fabricated for reference. The complete stack layer of the sample is shown in Fig. 1.

3. Preliminary measurements

Prior to the near field measurements, two preliminary tests were carried out to determine the experimental conditions in which the Super-RENS effect takes place. First, we used confocal microscopy to determine the laser intensity necessary to change the optical parameters of the sample, after being focused by the DVD lens. A single laser pulse with 1 ms duration and power higher than 4.0mW (equivalent to power density of $P_d \approx 7$mW/μm^2 in focus), caused a permanent modification of the optical parameters of the InSb sample. In other words, the sample is not able to restore its initial crystalline state after absorbing this amount of energy and as a result, a permanent mark will be formed. Within the range 1.0mW-4.0mW, the change in the optical parameters is reversible. This is the power range for which the Super-RENS effect takes place. Power values smaller than 1.0mW did not trigger any optical change. Analysis of the permanently formed marks at high power illumination conditions was performed by confocal

#162345 - $15.00 USD Received 1 Feb 2012; revised 24 Feb 2012; accepted 24 Feb 2012; published 20 Apr 2012

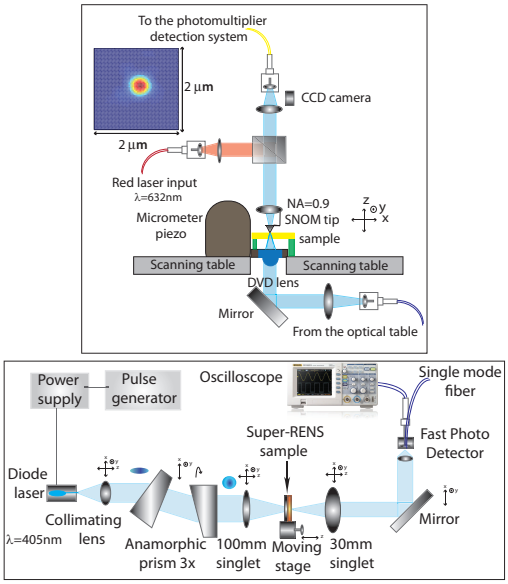

Fig. 2. Schematic diagram of the experimental setup. (bottom) Optical arrangement for generating a round shaped pulsed laser beam, which can be either used for time resolved measurements (in this case, the sample is placed on the moving stage and the transmitted signal collected by the Fast Photo Detector) or redirected to the SNOM measurement unit via a single mode optical fiber. Please notice that the Super-RENS sample is relocated to the SNOM microscope in this case. (top) Lightpath inside the SNOM microscope. The modified scanning table holds the DVD lens and the Super-RENS sample. Confocal microscopy is performed in reflection with a red laser source. Near-field measurements are taken with the SNOM tip in contact with the sample surface. An example of a measured focused spot can be seen on the top left.

microscopy for different focusing conditions. The shape of the permanently modified marks followed exactly the shape of the spot incident on the sample. The mark has a donut shape for a defocused spot and an approximately circular shape for a focused spot, as shown in Figs. 3(a) and 3(b), respectivelly. These observations confirm that the refractive index of the InSb material locally changes only above an intensity threshold and suggest that, in the power range where the Super-RENS takes place, the thermally-modified region will also follow the focused spot symmetry. Thus, for a circular symmetric focused spot, the modified area can be described by a cylinder, with height equal to the Super-RENS layer thickness and radius directly linked to the incident power. This description forms the basis for the threshold-like model that was established to describe the Super-RENS effect. More details of this model are presented in the next section.

In the following, the non-linear response of the InSb sample was investigated as a function of time to determine the incident pulse parameters required to trigger the Super-RENS effect. Square pulses of different width and 50% duty cycle were incident on the samples. In the case of the reference ZnS sample, the pulses were perfectly replicated in the detected signal, as shown by the blue curve in Fig. 4(a). In contrast, the InSb sample showed a non-linear response. As the thermally-modified area progressively increases in size, the laser intensity reaching the detector decreases by a factor of approximately 20%, until a stationary state is reached. At this point, the sample region illuminated by the focused spot becomes more absorbing/reflective than outside

#162345 - $15.00 USD Received 1 Feb 2012; revised 24 Feb 2012; accepted 24 Feb 2012; published 20 Apr 2012

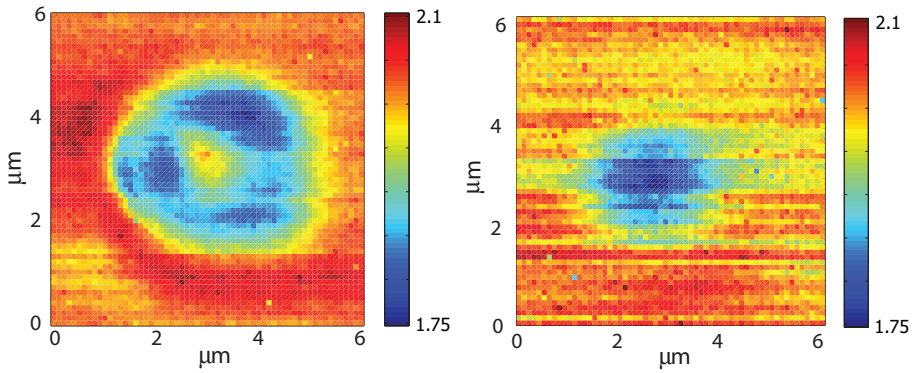

Fig. 3. Confocal microscopy measurements of the Super-RENS surface after permanently changing the optical parameters with a high intensity (a) defocused laser spot and (b) focused laser spot.

the illuminated region. As seen in Fig. 4(a), the stationary state is reached after approximately 120μs for a pulse of $\approx 3\text{mW}/\mu\text{m}^2$ incident on the sample. Considering that the radius of the focused spot from the DVD lens is about 40 times smaller than the spot focused by the lens used in the time resolved pump-probe setup (NA ≈ 0.1), we roughly estimate that the stationary state will be reached in about $120\mu\text{s}/40 \approx 3\mu$s in the actual Super-RENS measurements.

To verify the above prediction, the evolution of temperature as a function of time was calculated by solving the fundamental equation based on linear transient thermal conduction, Eq. 1,

$$\nabla^2 T(r,t) + \frac{1}{k} g(r,t) = \frac{1}{\alpha} \frac{\partial T(r,t)}{\partial t} \tag{1}$$

where, $\alpha = k/\rho C_p$ is the thermal diffusivity, k is the thermal conductivity coefficient ($4.45 W/m/^oC$), ρ is the density ($5760 kg/m^3$), C_p is the specific heat ($210 J/kg/^oC$), and T is the temperature. The source term, $g(r,t)$ gives the amount of heat energy per unit of time and volume generated in the InSb layer, and is proportional to the squared Airy function, $[J_1(\frac{2\pi NA}{\lambda} r)/(\frac{2\pi NA}{\lambda} r)]^2$ times the pulse time dependence, where J_1 is the Bessel function of first kind, NA = 0.6 and $\lambda = 405$nm. In this model, r is the radial direction, $r = r(x,y)$, and the z dependence of T was neglected. As initial boundary value conditions, we assumed $T(r,t=0) = 300K$ and $T(r = r_{max}, t) = 273K$. The values k, ρ, C_p and the proportionality constant were obtained from the reference [24]. The Eq. 1 was solved with a 2D Finite Element Method code implemented in Matlab environment.

The calculated temperature distribution for an infinitely long and thin InSb layer confirms the above prediction about the response time, as shown in Fig. 4(b). In conclusion, to trigger the Super-RENS effect, pulses with duration shorter than 3μs should be used. These considerations set the experimental illumination conditions to be used in §5 for the characterization of the Super-RENS focused spot by SNOM.

4. Threshold model

The confocal microscopy measurements have evidenced that the optical parameter change follows the focused spot symmetry, suggesting that the permittivity of the InSb layer can be con-

#162345 - $15.00 USD Received 1 Feb 2012; revised 24 Feb 2012; accepted 24 Feb 2012; published 20 Apr 2012

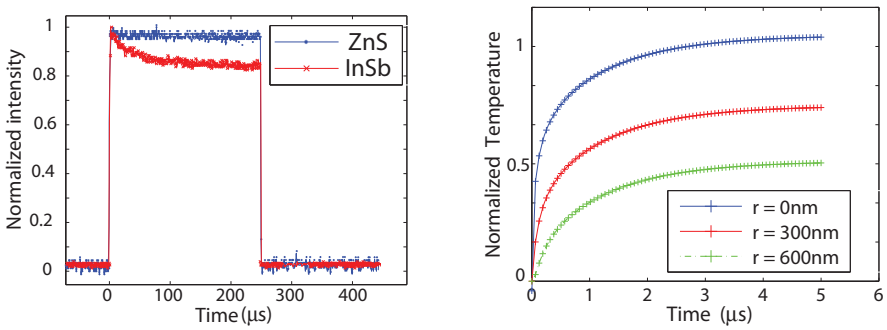

(a) (b)

Fig. 4. Time response of the Super-RENS InSb sample. (a) The measured linear response of the ZnS reference sample and the InSb sample for a single pulse with 250μs of duration. The decay observed for the InSb sample is due to the change in the optical parameters. (b) Simulated temperature distribution as function of time using an Airy focused spot as the heat source term. The temperature values were taken in the center of the focused spot (r= 0nm) and at radii r= 300*nm* and r= 600*nm*, normalized by the temperature value obtained at 5μs. A stationary state is reached after approximately 3μs.

sidered as a function of position, $\varepsilon = \varepsilon(x,y)$, to represent the local thermally-modified region. Thus, if the focused laser spot has circular symmetry, which can be generated by a circularly polarized plane wave at the entrance pupil of a lens with NA = 0.6, the thermally induced sub-wavelength region will also have circular symmetry. In other words, considering that the InSb layer is initially in its crystalline state, having a refractive index n_1, the refractive index will locally change from n_1 to n_2 under laser exposure in a region smaller than the focused spot total area. In practice, this region corresponds to a cylinder with radius r and height equal to the thickness of the super resolution layer. The radius r of the cylinder will increase as the laser power increases whereas a low intensity laser will not trigger the change of the refractive index at all. Figure 5 schematically explains the threshold model and shows the computational domain used in the 3D-FEM simulations. In all simulations, a cluster of four AMD Quad-Core Opteron F8354 (2.2GHZ) with 128Gb of internal memory, operating under Linux environment was used. Elements of order 2 were used on a hexahedral mesh with total size of $840 \times 840 \times 300$ nm^3. A perfectly matched layer with width of 80nm width in all directions was defined to truncate the computational domain. The number of unknowns could be as high as 800×10^3 and the total execution time of each calculation was about 5 hours.

As an example, Fig. 6(a) shows the normalized total electric field ($|E_t|^2 = |E_x|^2 + |E_y|^2 + |E_z|^2$) computed in the xz plane for the complete Super-RENS stack layer, in the presence of an optical scatterer with r= 50nm. The z-axis shows the position of each layer as they are defined in the computational domain. The color bar on the left side indicates the nature of each layer. The geometrical focal plane is chosen to be at z= 0nm, which lies inside the Super-RENS layer. From the computed electric field distribution, we plotted the intensity profile in the z plane 5nm below the ZnS-SiO_2/air boundary, as indicated by the dotted yellow line. This particular z-plane is chosen to allow comparisons with the near-field profiles measured experimentally with the SNOM microscope, since the probe will be in contact with the ZnS-SiO_2 layer. The electric field profile computed for different radii of the cylindrical region (r= 50nm, 170nm and 200nm) is displayed in the Fig. 6(b). When the scatterer region has a small radius, r= 50nm, a small portion in the central region of the incident spot where the intensity is the highest, will

#162345 - $15.00 USD Received 1 Feb 2012; revised 24 Feb 2012; accepted 24 Feb 2012; published 20 Apr 2012

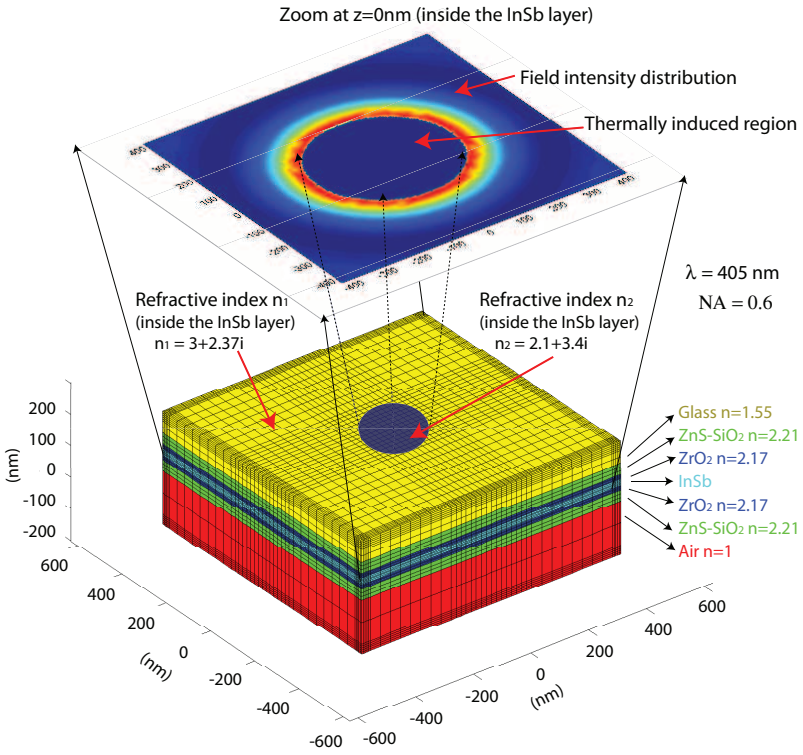

Fig. 5. Schematics of the threshold model and representation of the FEM computational domain. The Super-RENS effect is described by a local change in the refractive index of the super resolution material in a region inside the incident focused spot. This region is considered to be a cylinder with radius r and height equals to the thickness of the Super-RENS layer. The refractive index inside the cylinder is set to n_2. Outside the cylinder the refractive index remains n_1, corresponding to the refractive index of the InSb layer in its crystalline state. The 3D computational domain has size of $840 \times 840 \times 300\text{nm}^3$ with refined mesh in the portion where cylinder has to be represented. The refractive indices used, obtained from Ref. [25], are also provided.

#162345 - $15.00 USD Received 1 Feb 2012; revised 24 Feb 2012; accepted 24 Feb 2012; published 20 Apr 2012

be partially absorbing. The resulting spot profile after the Super-RENS layer will show a gap in its center, as seen in the blue curve (tagged with cross). As the radius of the scatterer region is increased, the gap in the spot profile disappears, resulting in a 'wing-shaped' profile (red curve, tagged with circles). At this point, the full width at half maximum (FWHM) of the spot is larger. For a sufficiently large scatterer region, the 'wings' will move downwards, leaving behind a spot profile with smaller FWHM.

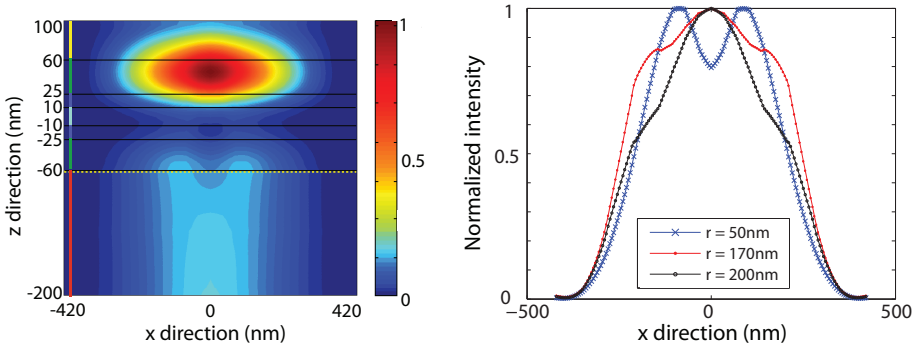

(a) (b)

Fig. 6. Finite element method simulation. (a) Distribution of the modulus of the total electric field computed for the Super-RENS stack in the presence of a r= 50nm scatterer region. (b) Modulus of the electric field profile computed in the plane represented by the dotted yellow line in (a) for scatterer regions with radius r= 50nm, r= 170nm and = 200nm.

5. Near-field Super-RENS spot measurements

The Super-RENS spot measurements were carried out in the near-field regime, i.e., with the SNOM probe in contact with the sample surface. In order to determine the best focus, a set of measurements were taken at different planes in the focal region. From the measurements, the smallest spot with highest intensity is considered to be the best focused spot. In the ideal case, the theoretical spot FWHM is in the order of $\lambda/2\text{NA}=340$nm. However, since the laser beam has a Gaussian profile on the entrance pupil of the DVD lens, the smallest experimental spot size measured in the reference ZnS-glass sample was found to be 380 ± 5nm whereas in the InSb sample (at low power), it was 376 ± 5nm. These values set the minimum focused spot size achievable in our setup when no Super-RENS effect was activated.

From the preliminary experiments reported in § 3, it is expected that the Super-RENS effect will occur for an incident laser power in the range of 1mW up to 4mW. In addition, the incident laser must be pulsed with duration below 3μs. Figure 7(a) shows the measured spot intensity distribution (normalized to unity) for the reference ZnS and for the InSb samples, with a 200ns pulsed laser at 2mW. The measured FWHM remains 380 ± 5nm for the ZnS sample and it decreases down to 290 ± 5nm for the InSb sample. Thus, a reduction of $\approx 25\%$ (100nm) in the spot FWHM due to the scatterer region formed in the InSb material is achieved. Figure 7(b) shows the normalized intensity profile of the two measured spots, taken at the dotted yellow line on the field maps. A 'needle-like' shape profile of the Super-RENS spot is found. This is, undoubtedly, a proof that the thermally-modified area in the scatterer-type Super-RENS layer does have direct influence on the focused spot profile and size. Hence, the occurrence of spot size reduction in scatterer-type Super-RENS materials is likely to be the main mechanism responsible for a readout signal beyond the diffraction limit.

#162345 - $15.00 USD Received 1 Feb 2012; revised 24 Feb 2012; accepted 24 Feb 2012; published 20 Apr 2012

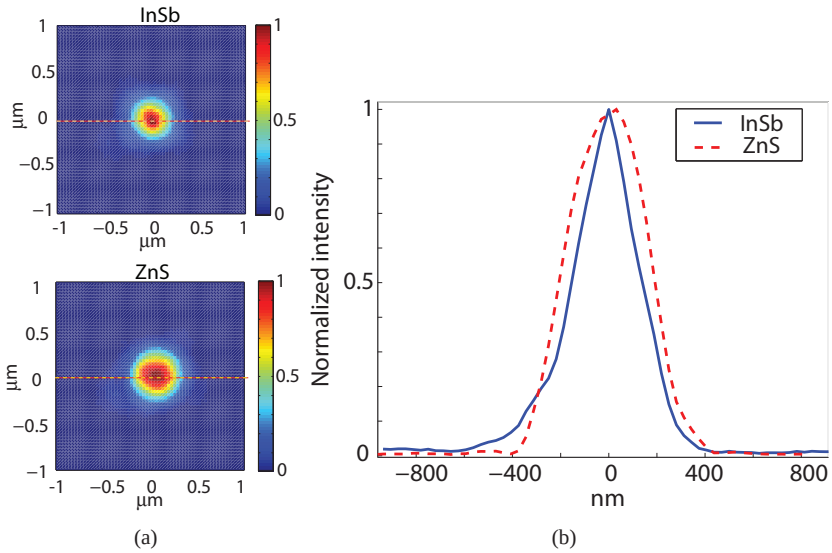

Fig. 7. Measured spots for the reference sample (ZnS) and the super resolution layer (InSb). (a) Spot intensity distribution measured for InSb and ZnS samples. (b) Intensity profile of (a). The Super-RENS focused spot is 100nm (in terms of FWHM) smaller when compared to the reference spot. Here, the pulsed laser beam has a duty cycle of 50%, with 200ns of duration and peak intensity of 2.0mW.

The experiments on Super-RENS discs conducted by Tominaga et al. [6] suggests that the laser power may directly influence the size of the modified focused spot. Under this consideration, we measured the FWHM as a function of the laser intensity, as shown by the black dotted curve tagged with filled stars in Fig. 8. For 200ns pulses, the spot size reduction associated with the Super-RENS effect occurred in the power range 1.3-3.5mW. The minimum spot size was 290nm at 1.8mW, and approximately 300nm in the power range 2.0-2.5mW. At higher power, it progressively increases again. At 4mW, no reduction is observed and the irreversible state of the Super-RENS layer is reached. A similar behavior was also observed at 250ns and 500ns pulses duration (not shown here). In all cases, nonetheless, a spot size with FWHM smaller than 300nm could be repetitively observed. In contrast, in the full power range measured, the spot focused on the ZnS reference sample had a constant FWHM of $\approx$ 375nm. For comparison between experiments and simulations, Fig. 8 also shows the simulated spot size computed as function of the scatterer radius (red line tagged with circles). The simulated spot size reaches a maximum value for r= 150nm and abruptly decreases afterwards. For r= 250nm, a minimum spot size is reached. As the scatterer radius increases to values larger than r= 250nm, the spot size gradually increases again. This behavior is in excellent agreement with the experimental results. In Figs. 9(a)-9(d) the measured and the simulated spot profiles used to extract the FWHM at the four positions, (a)-(d) indicated in the Fig. 8 are displayed. From Fig. 9(a), we notice that the 'wings' predicted by the threshold model are present in the measured spot, though they are less pronounced. Nevertheless, both measurement and simulation show a spot with large FWHM. At the position (b), plotted in Fig. 9(b), the peculiar 'winged' spot shape have moved downwards and at position (c) they have completely disappeared, leaving behind a spot size with smaller FWHM, as shown in Fig. 9(c). At this point, (c), both simulation and measurement show a very narrow focused spot. As the laser power increases, and the radius

#162345 - $15.00 USD Received 1 Feb 2012; revised 24 Feb 2012; accepted 24 Feb 2012; published 20 Apr 2012

of the thermally induced scatterer increases accordingly, the spot FHWM tends to increase as well, as shown in Fig. 9(d). In all cases, the simulated spots showed a very good agreement with the measured profiles, providing strong evidence that the threshold model is as a good approximation to describe the Super-RENS effect.

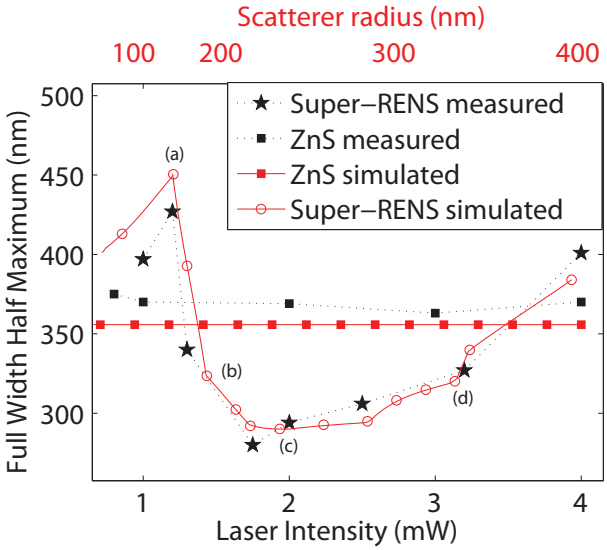

Fig. 8. Measured and simulated spot size as function of the laser power and scatterer radius, respectively, for a 200ns incident pulse length. A spot size reduction occurs for the scatterer-type of Super-RENS material in a certain laser power range. At this range, the measured spot size is not limited by diffraction. A good agreement between measurements and simulation is found.

6. Conclusion

In conclusion, we experimentally observed that the thermally-activated scatterer area generated in an InSb Super-RENS sample upon laser excitation has direct and noticeable influence on the focused spot size. Indeed, a reduction of the FWHM of 25% (100nm smaller than the limit of the setup) was measured. The unintuitive spot size reduction in scatterer-type Super-RENS material provides an explanation for the readout of data marks beyond the diffraction limit in optical discs. Moreover, the spot size dependence on parameters such as laser power and pulse width was verified. Experimental results suggest that the super-resolution effect can be modelled optically by a power threshold model. The implementation of the model in a 3D-FEM was shown, and the simulation results were found to be in excellent agreement with the experimental measurements. Therefore, this work contributes to improve the general understanding of the Super-RENS effect in the InSb materials as well as establishing ideas on which advanced microscopy, laser writing and lithography could take advantage.

We acknowledge support to this work by the FP7 European project IST-SURPASS, Project Number 224226.

#162345 - $15.00 USD Received 1 Feb 2012; revised 24 Feb 2012; accepted 24 Feb 2012; published 20 Apr 2012

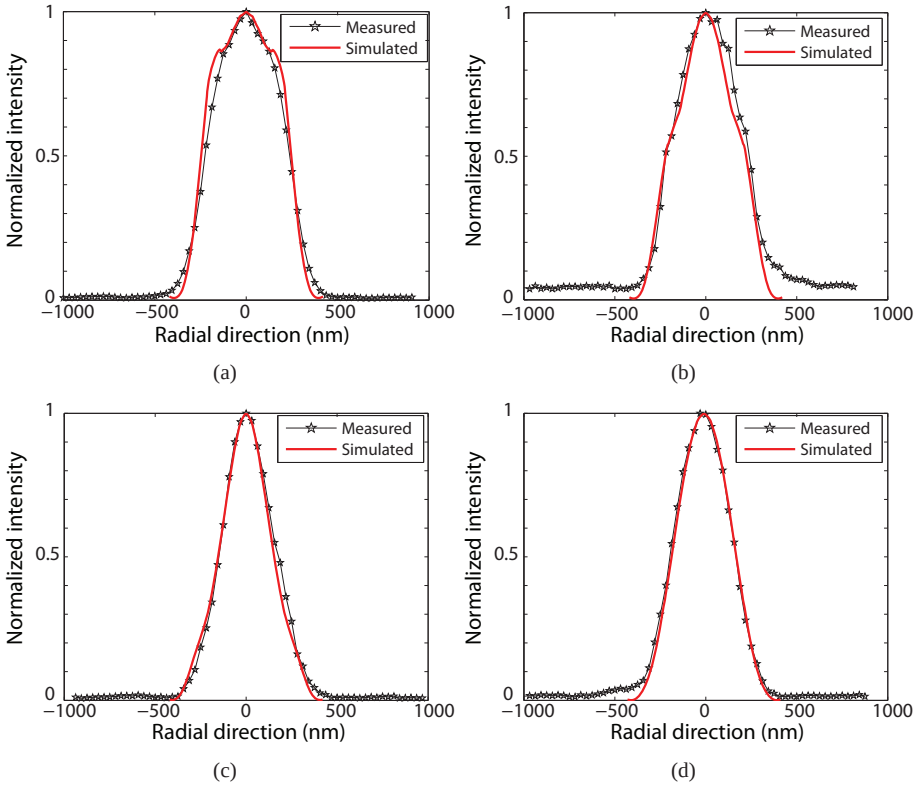

Fig. 9. Measured and simulated spot intensity profiles in the positions (a)-(d) indicated in the Fig. 8.

#162345 - $15.00 USD Received 1 Feb 2012; revised 24 Feb 2012; accepted 24 Feb 2012; published 20 Apr 2012